Radiosynthesis, Photoisomerization, Biodistribution, and Metabolite Analysis of ^{11}C-PBB3 as a Clinically Useful PET Probe for Imaging of Tau Pathology

Hiroki Hashimoto[1], Kazunori Kawamura[1], Nobuyuki Igarashi[1,2], Makoto Takei[1,2], Tomoya Fujishiro[1,2], Yoshiharu Aihara[1,2], Satoshi Shiomi[1,2], Masatoshi Muto[1,2], Takehito Ito[1,3], Kenji Furutsuka[1,3], Tomoteru Yamasaki[1], Joji Yui[1], Lin Xie[1], Maiko Ono[1], Akiko Hatori[1], Kazuyoshi Nemoto[1], Tetsuya Suhara[1], Makoto Higuchi[1], and Ming-Rong Zhang[1]

[1]Molecular Imaging Center, National Institute of Radiological Sciences, Chiba, Japan; [2]Tokyo Nuclear Services Co., Ltd., Tokyo, Japan; and [3]SHI Accelerator Service Ltd., Tokyo, Japan

2-((1*E*,3*E*)-4-(6-(¹¹C-methylamino)pyridin-3-yl)buta-1,3-dienyl) benzo[*d*]thiazol-6-ol (¹¹C-PBB3) is a clinically useful PET probe that we developed for in vivo imaging of tau pathology in the human brain. To ensure the availability of this probe among multiple PET facilities, in the present study we established protocols for the radiosynthesis and quality control of ¹¹C-PBB3 and for the characterization of its photoisomerization, biodistribution, and metabolism. **Methods:** ¹¹C-PBB3 was synthesized by reaction of the *tert*-butyldimethylsilyl desmethyl precursor (**1**) with ¹¹C-methyl iodide using potassium hydroxide as a base, followed by deprotection. Photoisomerization of ¹¹C-PBB3 under fluorescent light was determined. The biodistribution and metabolite analysis of ¹¹C-PBB3 was determined in mice using the dissection method. **Results:** ¹¹C-PBB3 was synthesized with 15.4% ± 2.8% radiochemical yield (decay-corrected, $n = 50$) based on the cyclotron-produced ¹¹C-CO_2 and showed an averaged synthesis time of 35 min from the end of bombardment. The radiochemical purity and specific activity of ¹¹C-PBB3 were 98.0% ± 2.3% and 180.2 ± 44.3 GBq/μmol, respectively, at the end of synthesis ($n = 50$). ¹¹C-PBB3 showed rapid photoisomerization, and its radiochemical purity decreased to approximately 50% at 10 min after exposure to fluorescent light. After the fluorescent light was switched off, ¹¹C-PBB3 retained more than 95% radiochemical purity over 60 min. A suitable brain uptake (1.92% injected dose/g tissue) of radioactivity was observed at 1 min after the probe injection, which was followed by rapid washout from the brain tissue. More than 70% of total radioactivity in the mouse brain homogenate at 5 min after injection represented the unchanged ¹¹C-PBB3, despite its rapid metabolism in the plasma. **Conclusion:** ¹¹C-PBB3 was produced with sufficient radioactivity and high quality, demonstrating its clinical utility. The present results of radiosynthesis, photoisomerization, biodistribution, and metabolite analysis could be helpful for the reliable production and application of ¹¹C-PBB3 in diverse PET facilities.

Key Words: tau pathology; Alzheimer disease; PET; ¹¹C-PBB3; photoisomerization

J Nucl Med 2014; 55:1532–1538
DOI: 10.2967/jnumed.114.139550

Accumulation of intracellular tau fibrils is a neuropathologic hallmark of Alzheimer disease (AD) and related tau-positive neurodegenerative disorders, which are collectively referred to as tauopathies (*1*). Understanding of the mechanistic roles played by pathologic tau in AD and related tauopathies has stimulated increasing interest in the development of imaging probes that facilitate visualization of tau pathology in the brains of living humans and animal models of tauopathies (*1*). ^{18}F-FDDNP (Fig. 1) was applied to PET imaging of intraneuronal neurofibrillary tangles for the first time (*2*). However, ^{18}F-FDDNP showed a relatively low contrast and selectivity for tau lesions versus β amyloid in in vitro autoradiograms and PET images of AD brains (*3*). In addition to ^{18}F-FDDNP, researchers have developed several promising PET probes for imaging tau protein in the brain (*4–10*). Among these radioprobes, ^{18}F-T807, ^{18}F-T808, ^{18}F-THK523, and ^{18}F-THK5105 (Fig. 1) have been used in clinical studies for AD patients (*6,8–10*), whereas its capability of capturing tau aggregates in non-AD tauopathies and transgenic animal models is yet to be determined.

Recently, we developed a new class of tau ligands, phenyl/pyridinyl butadienyl benzothiazoles/benzothiazoliums (PBBs). In vivo optical imaging of a transgenic mouse model demonstrated rapid and sensitive detection of intraneuronal tau inclusions by intravenous administration of these ligands, which are intrinsically fluorescent (*11*). Selected from these ligands, three ¹¹C-labeled compounds were synthesized and evaluated for their potential as PET probes for imaging tau pathology in tau transgenic mouse models (*11*). After preclinical evaluation, 2-((1*E*,3*E*)-4-(6-(¹¹C-methylamino)pyridin-3-yl)buta-1,3-dienyl)benzo[*d*]thiazol-6-ol (¹¹C-PBB3, Fig. 1) was applied to clinical PET studies and was demonstrated to effectively display tau pathology in patients with AD and non-AD tauopathies. Notably, the high-level retention of ¹¹C-PBB3 in the AD hippocampus wherein tau pathology is enriched sharply contrasted with that of a β-amyloid PET probe, ¹¹C-Pittsburgh compound B (¹¹C-PIB) (*11,12*).

Our previous study was focused on the development of PBBs and the application of ¹¹C-PBB3 to PET imaging of a mouse model and human brains (*11*). Meanwhile, the growing interest in the clinical use of ¹¹C-PBB3 in many PET facilities motivated us to establish protocols for its radiosynthesis and quality control and to characterize its chemical stability and its pharmacokinetic

Received Feb. 24, 2014; revision accepted May 19, 2014.
For correspondence or reprints contact: Ming-Rong Zhang, Molecular Probe Program, Molecular Imaging Center, National Institute of Radiological Sciences, 4-9-1 Anagawa, Inage-Ku, Chiba 263-8555, Japan.
E-mail: zhang@nirs.go.jp
Published online Jun. 24, 2014.

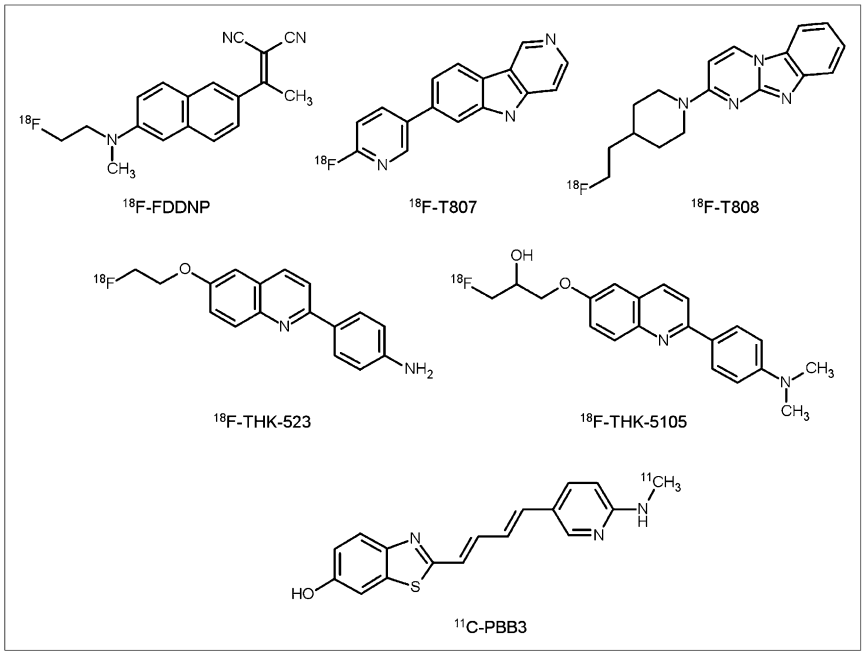

FIGURE 1. Chemical structures of PET probes for imaging of tau pathology in clinical use.

and metabolic properties. Here, we determined the radiosynthetic conditions for ^{11}C-PBB3 to obtain an appropriate amount of radioactivity with reliable quality for clinical application. Because of the chemical structure of pyridylbutadienylbenzothiazole in ^{11}C-PBB3, which is considered to easily undergo photoisomerization by exposure to ultraviolet light (*13*), we monitored the progress of photoisomerization of ^{11}C-PBB3 under fluorescent light and investigated how to prevent it during radiosynthesis and quality control. To validate whether the radioactive signals in the mouse and human brains were derived from ^{11}C-PBB3 itself, we performed metabolite analysis of ^{11}C-PBB3 for the mouse plasma and brain homogenate.

MATERIALS AND METHODS

General

PBB3 and its precursor (5-((1*E*,3*E*)-4-(6-(*tert*-butyldimethylsilyloxy)-benzo[*d*]thiazol-2-yl)buta-1,3-dienyl)pyridin-2-amine (**1,** Fig. 2) for radiosynthesis were synthesized and supplied from the NARD Institute. Commercially available reagents and organic solvents (Sigma-Aldrich and Wako Pure Chemical Industries) were used without further purification. ^{11}C was produced by ^{14}N (p, α)^{11}C nuclear reaction using a CYPRIS HM18 cyclotron (Sumitomo Heavy Industries). Effluent radioactivity was monitored using a NaI (Tl) scintillation detector system (Gabi Star PET; Raytest). If not otherwise stated, radioactivity was determined using an IGC-3R Curiemeter (Aloka).

Male ddY mice were purchased from Japan SLC Inc. Animals were maintained and handled in accordance with the recommendations of the U.S. National Institutes of Health and the guidelines of the National Institute of Radiologic Sciences. Animal experiments were approved by the Animal Ethics Committee of the National Institute of Radiologic Sciences. Male ddY mice (35.2 ± 2.2 g) were fed ad libitum.

Radiosynthesis of ^{11}C-PBB3

^{11}C-methyl iodide (^{11}C-CH_3I) was synthesized from cyclotron-produced ^{11}C-CO_2 using an automated synthesis system developed in-house (*14*). The produced ^{11}C-CH_3I was trapped in a mixture of the *tert*-butyldimethylsilyl group-protected desmethyl precursor **1** (0.9–1.1 mg) in anhydrous dimethylsulfoxide (0.15 mL) and KOH (10 mg) suspended in anhydrous dimethylsulfoxide (0.3 mL) at room temperature. Heating the reaction mixture at 125°C for 5 min produced 5-((1*E*,3*E*)-4-(6-(*tert*-butyldimethylsilyloxy)benzo[*d*]thiazol-2-yl)buta-1,3-dienyl)-*N*-2-^{11}C-methylpyridin-2-amine (^{11}C-**2**). Subsequent deprotection of the *tert*-butyldimethylsilyl group in ^{11}C-**2** was performed using H_2O (0.2 mL) at 50°C for 2 min. After 1.5 mL of the high-performance liquid chromatography (HPLC) solvent was added to the reaction vessel, the radioactive mixture was loaded into a preparative HPLC system (Jasco) for separation. The HPLC conditions were as follows: Atlantis T3 (5 μm, 10-mm internal diameter [i.d.] × 150 mm; Waters); acetonitrile/50 mM sodium phosphate buffer (pH 7.0) (20/30, v/v); 6.0 mL/min; 379-nm ultraviolet light. The fraction corresponding to ^{11}C-PBB3 (retention time [t_R], ~7 min) was collected into a flask in which 25% ascorbic acid (0.4 mL) and polysorbate-80 (0.075 mL) in ethanol (0.3 mL) had been added before radiosynthesis, and was then evaporated to dryness. The residue was dissolved in physiologic saline (6–12 mL) and sterilized with a Millex-GS filter (Millipore). An amber vial was filled with the formulated product.

All radiosynthesis and subsequent quality control procedures were performed without fluorescent light to prevent photoisomerization of ^{11}C-PBB3. If necessary, an ultraviolet-cutoff flashlight (green light, LED-41VIS525; OptoCode) was used to monitor these procedures for a short time.

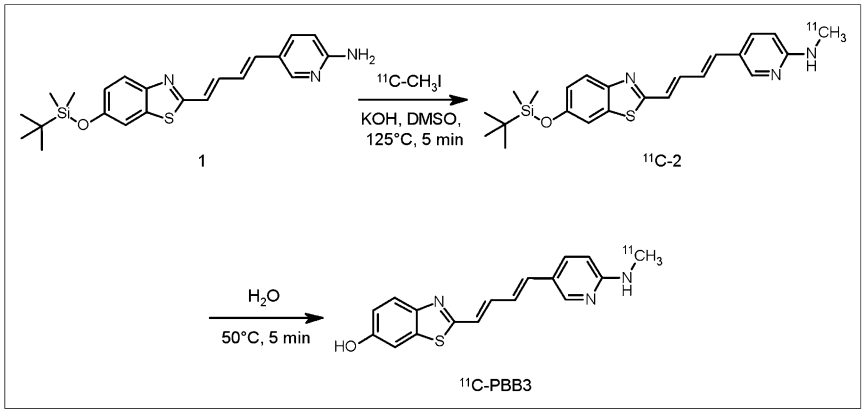

FIGURE 2. Radiosynthesis of ^{11}C-PBB3.

Determination of Radiochemical Purity and Photoisomerization

With the fluorescent light switched off, the final product solution of ^{11}C-PBB3 was analyzed using an HPLC system (515 pump and 2487 ultraviolet detector; Waters) and an XBridge Shield RP18 column (2.5 μm, 3.0 mm i.d. × 50 mm; Waters). A mixture of 90%

aqueous acetonitrile and 50 mM ammonium phosphate buffer (pH 9.3) (50/50 [0–1.2 min] and then 70/30 [1.2 min and onward], v/v) was used as the mobile phase. The t_R of ^{11}C-PBB3 was approximately 1.1 min at 1.0 mL/min. The identity was confirmed by coinjection with an authentic PBB3 sample. The specific activity was calculated by comparison of the assayed radioactivity to the carrier mass, which was measured on the basis of its ultraviolet peak at 379 nm. To determine the radiochemical stability of ^{11}C-PBB3, the formulated product was maintained for 60 min at room temperature without fluorescent light. An analytic sample was taken from the formulated solution to measure the radiochemical purity again.

For comparison, a portion of the ^{11}C-PBB3 injection sample was transferred to a colorless vial and maintained for 60 min at room temperature under fluorescent light. Analytic samples were taken from this vial to measure the radiochemical purity at 1, 10, and 60 min.

Quality Control

In addition to determination of radiochemical purity and specific activity, the physical appearance of the ^{11}C-PBB3 injection was checked by visual inspection (*15*). pH was measured using a pH meter (F-71; Horiba) and a probe (9618-10D; Horiba). Sterility was tested using a soybean-casein digest broth (Merck) incubated with the injection sample at 20°C–25°C for 14 d and fluid thioglycollate medium (Merck) incubated with the sample at 30°C–35°C for 14 d. Absence of culture growth after 14 d indicates sterility (*16*). The endotoxin content in the injection sample was measured using a toxinometer (ET-6000; Wako) (*17*). Residual organic solvents (acetonitrile and ethanol) were measured using a gas chromatography system (7890; Agilent Technologies) (*18*). A DB-WAX column (0.50 μm, 0.53-mm i.d. × 30 m; Agilent Technologies) was maintained at 40°C (0–8 min), raised to 120°C (8–28 min), and kept at 120°C (28–33 min). The makeup gas was nitrogen (99.9995%, 50 mL/min), and the carrier gas was helium (99.995%, 4 mL/min). A flame ionization detector was used.

Biodistribution Study

^{11}C-PBB3 (1.6 MBq in 0.1 mL, 49.6 GBq/μmol) was injected into the tail vein of mice (n = 4 for each time point) without fluorescent light. The blood, heart, lung, spleen, liver, small intestine, testis, kidney, muscle, and brain were dissected at 1, 5, 15, 30, and 60 min after injection. The radioactivity in each tissue was measured using a γ counter (1480 Wizard 3; Perkin-Elmer) and expressed as follows: uptake [percentage injected dose (%ID)/g] = [tissue radioactivity (cps) × 100/tissue weight (g)]/injected dose (cps). All measured radioactivity values were corrected for decay.

Metabolite Analysis in Brain and Plasma

^{11}C-PBB3 (33.3–37 MBq in 0.1–0.2 mL, 51.9 ± 18.2 GBq/μmol) was injected into the tail vein of mice (n = 3 for each time point), and the mice were sacrificed by cervical dislocation at 1 and 5 min after injection. Blood samples were obtained and centrifuged at 15,000 rpm for 1 min at 4°C. The plasma (0.5 mL) was separated and transferred to a tube containing acetonitrile (0.5 mL). The mixture was stirred in a vortex mixer and centrifuged at 15,000 rpm for 2 min to separate the precipitate from the aqueous phase.

The half brain was placed in test tubes, each containing 2.5 mL of ice-cooled saline, and homogenized (SilentCrusher-S; Heidolph Instruments). Radioactivity (%ID/g) in the left brain was measured at the same time. The homogenized brain tissue (0.5 mL) was transferred to a tube containing acetonitrile (0.5 mL) and centrifuged (15,000 rpm, 2 min, 4°C). The precipitate and supernatant were separated and measured for radioactivity. The supernatants of the plasma and brain homogenates were analyzed using an HPLC system equipped with a highly sensitive detector for radioactivity (*19*). The HPLC system and conditions were as follows: pump, PU-2089 plus (Jasco); ultraviolet detector, UV-2075 (Jasco); NaI(Tl) scintillation detector (S-2493A; OKEN); precolumn, XBridge Prep C18 Guard Cartridge (5 μm, 10 mm i.d. × 10 mm; Waters); main column, XBridge OST C18 (2.5 μm, 10 mm i.d. × 50 mm; Waters); mobile phase, 90% aqueous acetonitrile/0.02 M sodium phosphate buffer (pH 7.0) (30/70 [0–4 min], 40/60 to 70/30 [4–7 min], v/v); flow rate, 8.0 mL/min; t_R, ^{11}C-PBB3, 5 min. All the procedures in this section were conducted with the fluorescent light switched off.

RESULTS

Radiosynthesis of ^{11}C-PBB3

^{11}C-PBB3 was synthesized by *N*-methylation of the desmethyl precursor **1** with ^{11}C-CH_3I using KOH as a base (Fig. 2), followed by deprotection of the *tert*-butyldimethylsilyl group in the intermediate ^{11}C-**2** with water. After the reaction, HPLC separation (Fig. 3), and formulation, ^{11}C-PBB3 was successfully obtained with a sufficient amount of radioactivity. At the end of synthesis, ^{11}C-PBB3 of 1.6–3.1 GBq was obtained as an injectable solution of sterile normal saline after 30–35 min of proton bombardment at a beam current of 18 μA. The decay-corrected radiochemical yield of ^{11}C-PBB3 based on ^{11}C-CO_2 was 15.4% ± 2.8% (n = 50) at the end of bombardment, and the specific activity was 180.2 ± 44.3 GBq/μmol (n = 50) at the end of synthesis. The averaged radiochemical purity of the ^{11}C-PBB3 product in an amber vial was 98.0% ± 2.3% (Fig. 4A) and remained greater than 95% after 60 min (Fig. 4B) without fluorescent light. The total synthesis time was approximately 35 min from the end of bombardment.

Photoisomerization

Figures 4C–4E show the photoisomerization of ^{11}C-PBB3 in a colorless vial under fluorescent light. At 1 min after exposure to the fluorescent light, the radiochemical purity of ^{11}C-PBB3 decreased to 77%. From 10 to 60 min, its radiochemical purity remained approximately 50%. The chemical structure of the ^{11}C-impurity was not identified but was assumed to be the *Z, Z* or *E, Z* isomer of ^{11}C-PBB3.

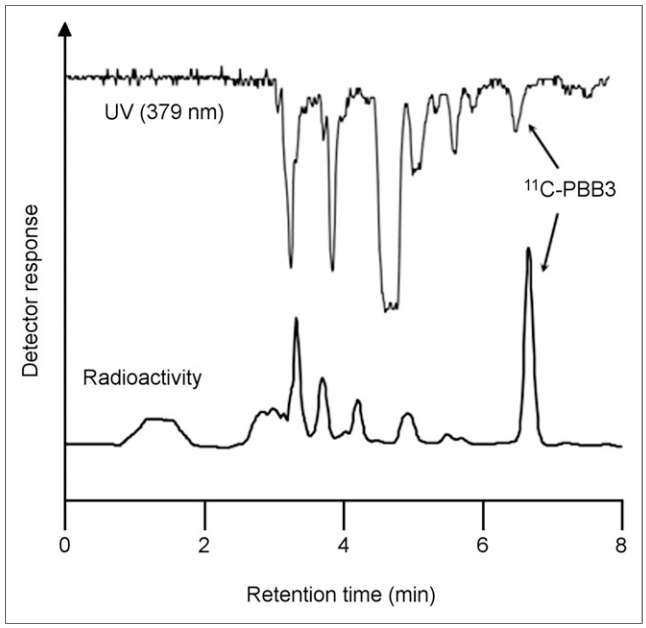

FIGURE 3. Typical preparative HPLC chromatogram of ^{11}C-PBB3.

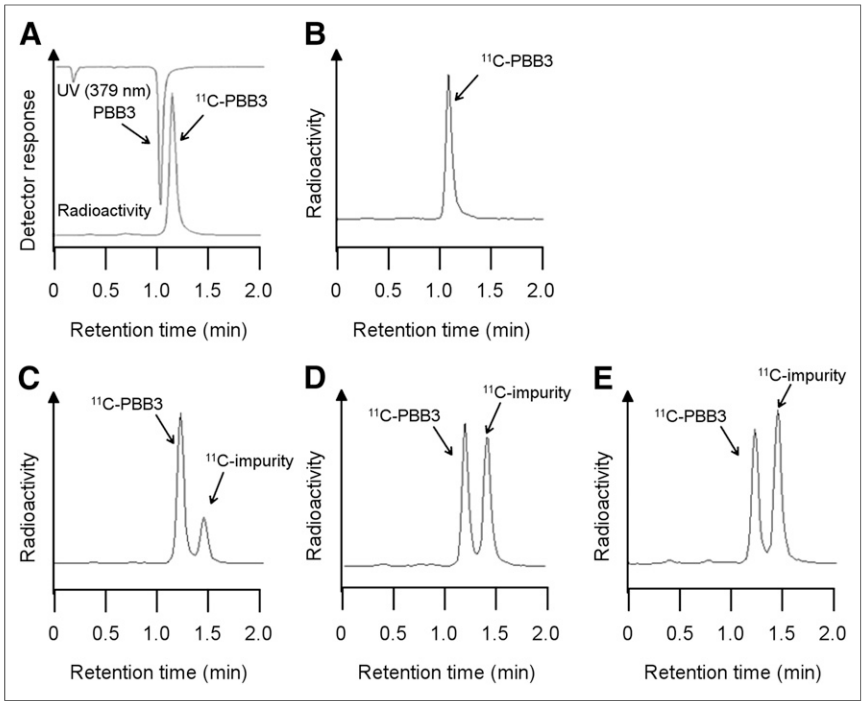

FIGURE 4. Typical analytic HPLC chromatograms of ^{11}C-PBB3. Analyses were performed without (A and B) and with (C–E) fluorescent light. Identity of ^{11}C-PBB3 was confirmed by co-injection with authentic PBB3 sample immediately after formulation (A) and at 60 min (B), 1 min (C), 10 min (D), and 60 min (E).

Quality Control

Table 1 summarizes the results of the quality control assessment for 3 different lots of ^{11}C-PBB3 production. The physical appearance of the product was clear and without particles. The pH was 6.7 ± 0.8. In sterility testing, no viable bacteria or microorganisms were observed in soybean-casein digest broth or fluid thioglycollate medium. The endotoxin content was undetectable (<0.7 endotoxin units/maximum volume). The radiochemical purity of ^{11}C-PBB3 was 98.2% ± 2.2% (n = 3) at the end of synthesis and was within the range of 97.0% ± 0.8% after 60 min. The residual amounts of ethanol and acetonitrile in the ^{11}C-PBB3 injection sample were to be 6.7 ± 0.6 ppm and 1 ppm, respectively.

Biodistribution Study

Table 2 shows the tissue distribution of radioactivity in the whole body of mice at 1, 5, 15, 30, and 60 min after injection of ^{11}C-PBB3. Uptake in most tissues was the highest at 1 min among all sampling time points. The radioactivity levels in the blood, heart, lung, testis, muscle, and brain decreased rapidly after initial uptake, whereas the radioactivity in the liver, spleen, small intestine, and kidney reduced gradually after 5 min. The radioactivity in all tissues except the small intestine cleared to less than 1 %ID/g at 60 min. Brain uptake was 1.92 %ID/g at 1 min and then decreased rapidly to 0.03 %ID/g at 60 min.

Metabolite Analysis in Brain and Plasma

Figure 5 shows the HPLC chromatograms for the plasma and brain homogenate samples after injection of ^{11}C-PBB3. In the plasma, the percentage of ^{11}C-PBB3 rapidly decreased and a radiolabeled metabolite was observed as early as 1 min after injection (Fig. 5A). The fraction corresponding to unchanged ^{11}C-PBB3 in the plasma was 1.9% ± 0.53% at 5 min (Fig. 5B) and was not detectable at 15 min (data not shown). The radiolabeled metabolite was more polar than ^{11}C-PBB3, as estimated by its t_R (2.0 min) on the HPLC charts. Despite the rapid metabolism in plasma, the percentage of unchanged ^{11}C-PBB3 in the brain homogenate was 82% at 1 min (Fig. 5C) and 70% at 5 min (Fig. 5D). A radiolabeled metabolite was also detected in the HPLC charts of the brain samples, and its t_R was similar to that of the metabolite in the plasma. Calculated from the total brain uptake (%ID/g), which was simultaneously measured for the same mice, radioactivity levels representing unchanged ^{11}C-PBB3 and ^{11}C-metabolite in the brain were found to be 1.58 ± 0.25 and 0.35 ± 0.06 %ID/g, respectively, at 1 min and 0.83 ± 0.06 and 0.35 ± 0.04 %ID/g, respectively, at 5 min. Recovery of radioactivity from HPLC analysis for all samples was greater than 95%. Because of the low

TABLE 1
Quality Control for ^{11}C-PBB3 Productions (n = 3)

Test	Acceptance criterion	Lot 1	Lot 2	Lot 3
Radioactivity (GBq)	Not less than 0.185	1.56	1.88	1.82
Specific activity (GBq/μmol)	Not less than 3.7	141.2	186.6	138.2
Bacterial endotoxin (international units/maximum dose)	<175	<0.5	<0.5	<0.5
Sterility	No bacterial growth	No bacterial growth	No bacterial growth	No bacterial growth
pH	4.5–8.0	6.8	6.6	6.8
Radiochemical purity after 60 min	Not less than 95% of total radioactivity	96.1%	97.5%	97.5%
Residual solvent (ppm)				
Ethanol	<5,000	7	6	7
Acetonitrile	<410	1	1	1

TABLE 2
Biodistribution for ^{11}C-PBB3 in Mice

Site	1 min	5 min	15 min	30 min	60 min
Blood	4.34 ± 0.38	3.06 ± 0.65	1.27 ± 0.19	0.64 ± 0.12	0.12 ± 0.03
Heart	5.98 ± 0.72	2.10 ± 0.17	0.72 ± 0.07	0.32 ± 0.03	0.06 ± 0.02
Lung	12.51 ± 1.06	3.58 ± 2.46	2.12 ± 0.20	1.07 ± 0.28	0.21 ± 0.07
Spleen	1.62 ± 0.40	3.49 ± 2.48	0.43 ± 0.03	0.23 ± 0.07	0.07 ± 0.01
Liver	8.01 ± 1.01	14.81 ± 1.29	9.01 ± 1.04	4.42 ± 0.76	0.88 ± 0.17
Small intestine	14.71 ± 3.97	45.58 ± 7.82	29.64 ± 8.02	16.72 ± 5.34	3.57 ± 1.44
Testis	0.56 ± 0.09	1.15 ± 0.54	0.68 ± 0.22	0.47 ± 0.10	0.09 ± 0.01
Kidney	12.49 ± 1.19	10.55 ± 0.81	4.36 ± 0.40	1.80 ± 0.26	0.30 ± 0.05
Muscle	2.59 ± 0.25	1.33 ± 0.23	0.55 ± 0 .07	0.22 ± 0.02	0.04 ± 0.04
Brain	1.92 ± 0.13	0.97 ± 0.06	0.27 ± 0.02	0.11 ± 0.04	0.03 ± 0.01

Data are mean (± SD) %ID/g tissue (n = 4).

radioactivity level, no further metabolite analysis was performed for the brain samples collected beyond 5 min.

DISCUSSION

In this study, ^{11}C-PBB3, a PET probe clinically used for imaging tau pathology in the human brain, was reliably synthesized with sufficient radioactivity and high quality. The metabolite analysis demonstrated the presence of unchanged ^{11}C-PBB3 as the major radiolabeled component in the mouse brain despite its rapid metabolism in the plasma.

For the radiosynthesis of ^{11}C-PBB3, the *tert*-butyldimethylsilyl group-protected desmethyl compound **1** was designed as the precursor. ^{11}C-methylation of **1** and subsequent deprotection of ^{11}C-**2** gave ^{11}C-PBB3 in a 2-step, 1-pot process (Fig. 2). We initially attempted to perform ^{11}C-methylation of **1** using ^{11}C-CH_3OTf and no base, as is done for the synthesis of ^{11}C-Pittsburgh compound B, which was easily labeled by direct ^{11}C-methylation without requiring a base (*20*). However, this approach could not produce ^{11}C-**2,** indicating that the α-amino group in the pyridine ring of **1** did not have enough nucleophilicity to undergo ^{11}C-methylation without a base. Use of organic bases gave only trace amounts of ^{11}C-**2.** Because the low labeling efficiency with ^{11}C-CH_3OTf without a base could not be improved even by heating the reaction mixture to 150°C for 5 min, this approach was not pursued further.

We then used KOH powder as a base to form the salt of the amine group in situ for the ^{11}C-methylation of **1** with ^{11}C-CH_3I. The reaction conditions, including the amount of KOH, reaction solvent, time, and temperature, were optimized. It was found that the use of 10 mg of KOH, which was suspended in anhydrous dimethylsulfoxide for 20–30 s with an ultrasonic cleaner just before the synthesis, for reaction of 1 mg of **1** with ^{11}C-CH_3I at 125°C for 5 min could give the highest yield of ^{11}C-**2.**

To remove the protective *tert*-butyldimethylsilyl group in ^{11}C-**2,** we initially used tetrabutylammonium fluoride. Although the deprotection was successful, perfect removal of tetrabutylammonium fluoride and its decomposing residues in the final formulated product remained challenging. In place of tetrabutylammonium fluoride, we then used water to remove the *tert*-butyldimethylsilyl group. As expected, deprotection

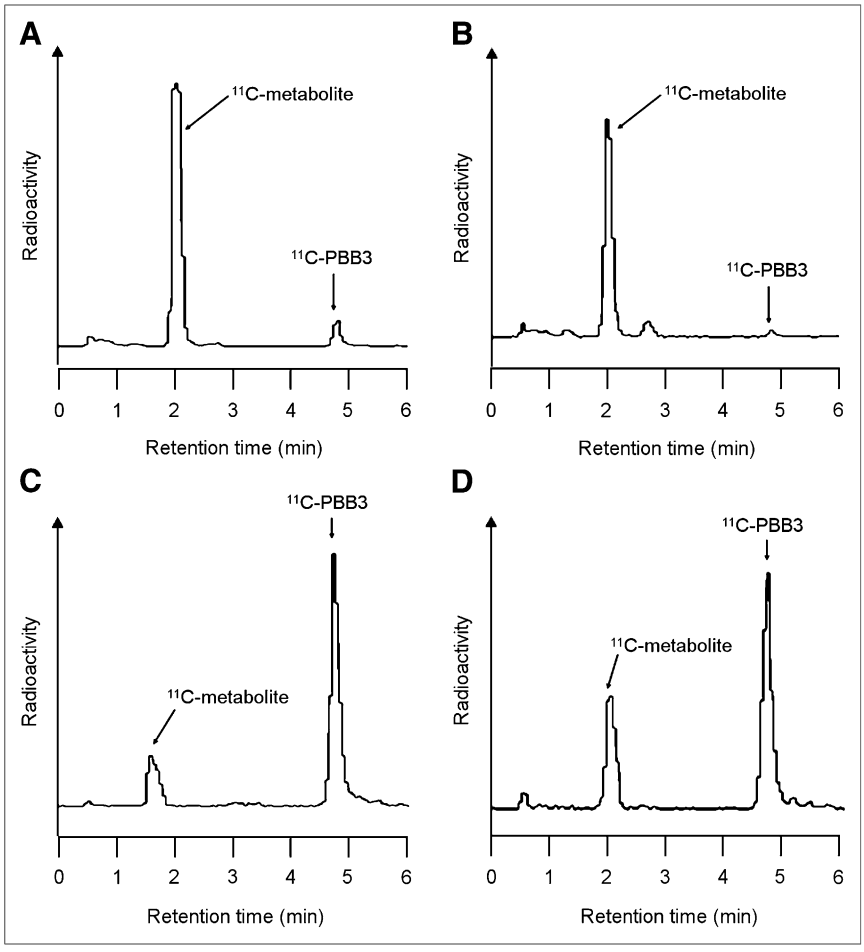

FIGURE 5. HPLC chromatograms for metabolite analysis of ^{11}C-PBB3 at 1 min in mouse plasma (A), at 5 min in mouse plasma (B), at 1 min in mouse brain (C), and at 5 min in mouse brain (D).

with alkali water at 50°C for 2 min proceeded perfectly. Indeed, alkali water was also used to remove the *tert*-butyldimethylsilyl group in the synthesis of ^{11}C-AZD2184, an imaging agent for β amyloid with structural similarity to ^{11}C-PBB3 (*21*).

Photoisomerization is a molecular behavior in which a structural change between isomers occurs because of photoexcitation. *E* and *Z* conversion is a representative behavior. Chemicals exhibiting this conversion include stilbene and azobenzene, in which the rotation or inversion around the double bond affords the isomerization between the 2 states (*13*). ^{11}C-PBB3 underwent rapid photoisomerization as a pyridylbutadienylbenzothiazole compound by exposure to fluorescent light as shown in the analytic HPLC charts (Figs. 4C–4E). Compared with ^{11}C-PBB3, its ^{11}C-isomer showed much less specific binding to tau in the brain sections of AD patients (Supplemental Fig. 1; supplemental materials are available at http://jnm.snmjournals.org). This photoisomerization could be prevented by switching off the fluorescent light. By cutting off all fluorescent light in the synthetic hot cell to perform the radiosynthesis, in particular HPLC separation and formulation, and using an amber vial to store the formulated product, ^{11}C-PBB3 was reliably obtained with high radiochemical purity without isomerization and radiolysis. All the results of quality control for the ^{11}C-PBB3 injection complied with our in-house quality control and quality assurance specifications (Table 1). These data have guaranteed a reliable supply of ^{11}C-PBB3 with sufficient radioactivity and high quality for clinical application.

The results of the biodistribution study of ^{11}C-PBB3 in mice suggest that the radioactivity might be cleared mainly via the hepatobiliary and intestinal reuptake pathways, with rapid washout from the body (Table 2). The present brain uptake indicates that ^{11}C-PBB3 easily passed through the blood–brain barrier, which is related to its lipophilicity (calculated logD, 3.30) (*11*). The effective dose estimate for ^{11}C-PBB3 was 3.28 μSv/MBq (Supplemental Table 1), which was comparable to that reported for other ^{11}C-labeled probes, including ^{11}C-Pittsburgh compound B (4.7 μSv/MBq) (*22*).

Metabolite analysis demonstrated that this probe was rapidly decomposed to a polar radiolabeled metabolite in the plasma (Fig. 5). Despite the high abundance in the plasma, this metabolite, which was more hydrophilic than ^{11}C-PBB3, showed limited entry into the brain. This finding indicates that uptake of radioactivity into the mouse brain was attributable mainly to unchanged ^{11}C-PBB3. The present data, taken together with the results of the previous metabolite analysis for human plasma (*11*), demonstrated that ^{11}C-PBB3 is rapidly metabolized to the same radiolabeled metabolite in mouse and human plasma, as evidenced by the similar t_Rs in the HPLC charts for plasma samples from these 2 species. The percentage of unchanged ^{11}C-PBB3 in human plasma at 3 min after injection was 7.8% ± 2.2%, and the metabolizing rate in human plasma was slightly slower than that in mouse plasma. These results indicate that the radioactive signals acquired by PET in the human brain may primarily reflect the kinetics of ^{11}C-PBB3. However, the influence of the low-grade uptake of radioactive metabolites into the brain on pharmacokinetic measures of ^{11}C-PBB3 should be clarified.

In both humans and mice, the rapid entry of ^{11}C-PBB3 into the brain and prompt reduction of the parent probe in the plasma imply that the levels of ^{11}C-PBB3 in the brain may be dependent largely on its first-pass extraction (*11*). This characteristic, along with its minimal nonspecific binding of ^{11}C-PBB3 to the myelin-rich components (*11*), resulted in a rapid washout of this probe from the brain, thereby reducing the background signal in the brain. Moreover, the significant contribution of the first-pass extraction to the radioprobe kinetics in the brain indicates that regional cerebral blood flow may be a critical determinant of the amount of ^{11}C-PBB3 entering the brain; accordingly, the specific binding of ^{11}C-PBB3 to tau lesions may be underestimated in areas with profound hypoperfusion. In fact, PET imaging with ^{11}C-PBB3 in the AD brain displayed high-contrast signals in the hippocampus and low nonspecific retention in the white matter and other myelin-rich regions (*11*). Although the brain uptake of ^{11}C-PBB3 is lower than that of ^{18}F-T807 and ^{11}C-Pittsburgh compound B (*5,11,23*), a relatively low concentration of free ^{11}C-PBB3 in the brain may be advantageous to its selective binding to high-affinity, low-capacity sites on tau fibrils, compared with the low-affinity, high-capacity binding sites on β amyloid (*11*).

A shortcoming of ^{11}C-PBB3 may be the presence of the radiolabeled metabolite in the mouse brain, although brain uptake of this metabolite was lower than that of unchanged ^{11}C-PBB3 in the brain. Determination of the metabolic pathway for ^{11}C-PBB3 is currently ongoing and should provide clues for the design of new probes with improved biostability. Identification of the chemical structure of the major ^{11}C-PBB3 metabolite should also be performed, and subsequent radiolabeling of this metabolite would facilitate evaluation of its plasma and brain kinetics and affinity for tau fibrils.

CONCLUSION

^{11}C-PBB3, a clinically useful PET probe for tau pathology in the brains of humans and transgenic mouse models, was successfully synthesized by reaction of *tert*-butyldimethylsilyl desmethyl precursor **1** with ^{11}C-CH_3I in the presence of KOH, followed by deprotection with water. We have so far achieved more than 200 productions of ^{11}C-PBB3 in our facility for various research purposes, including translational PET imaging of mouse models and clinical PET assessments of patients diagnosed as having AD and non-AD neurodegenerative disorders. The present results demonstrate the reliable production and widespread clinical potential of ^{11}C-PBB3.

DISCLOSURE

The costs of publication of this article were defrayed in part by the payment of page charges. Therefore, and solely to indicate this fact, this article is hereby marked “advertisement” in accordance with 18 USC section 1734. This study was funded in part by Grants-in-Aid for the Japan Advanced Molecular Imaging Program, Scientific Research (B) (23390235), Core Research for Evolutional Science and Technology, and Scientific Research on Innovative Areas (Brain Environment) (23111009) from the Ministry of Education, Culture, Sports, Science, and Technology, Japan. Drs. Suhara, Higuchi, and Zhang are named as inventors on patent application 0749006WO1, claiming subject matter related to the results described in this paper. No other potential conflict of interest relevant to this article was reported.

REFERENCES

1. Ballatore C, Lee VMY, Trojanowski JQ. Tau-mediated neurodegeneration in Alzheimer’s disease and related disorders. *Nat Rev Neurosci.* 2007;8:663–672.
2. Small GW, Kepe V, Ercoli LM, et al. PET of brain amyloid and tau in mild cognitive impairment. *N Engl J Med.* 2006;355:2652–2663.
3. Thompson PW, Ye L, Morgenstern JL, et al. Interaction of the amyloid imaging tracer FDDNP with hallmark Alzheimer’s disease pathologies. *J Neurochem.* 2009;109:623–630.

4. Villemagne VL, Furumoto S, Fodero-Tavoletti M, et al. The challenges of tau imaging. *Future Neurol.* 2012;7:409–421.
5. Baskin A, Giannakopoulos P, Ratib O, et al. PET radiotracers for molecular imaging in dementia. *Curr Radiopharm.* 2013;6:215–230.
6. Chien DT, Bahri S, Szardenings AK, et al. Early clinical PET imaging results with the novel PHF-tau radioligand [F-18]-T807. *J Alzheimers Dis.* 2013;34: 457–468.
7. Ballatore C, Smith AB III, Lee VM, et al. Aminothienopyridazines as imaging probes of tau pathology: a patent evaluation of WO2013090497. *Expert Opin Ther Pat.* 2014;24:355–360.
8. Chien DT, Szardenings AK, Bahri S, et al. Early clinical PET imaging results with the novel PHF-tau radioligand [F-18]-T808. *J Alzheimers Dis.* 2014;38: 171–184.
9. Fodero-Tavoletti MT, Furumoto S, Taylor L, et al. Assessing THK523 selectivity for tau deposits in Alzheimer's disease and non Alzheimer's disease tauopathies. *Alzheimers Res Ther.* 2014;6:11.
10. Okamura N, Furumoto S, Fodero-Tavoletti MT, et al. Non-invasive assessment of Alzheimer's disease neurofibrillary pathology using ^{18}F-THK5105 PET. *Brain.* 2014;137:1762–1771.
11. Maruyama M, Shimada H, Suhara T, et al. Imaging of tau pathology in a tauopathy mouse model and in Alzheimer patients compared to normal controls. *Neuron.* 2013;79:1094–1108.
12. Wood H. Alzheimer disease: [^{11}C]PBB3—a new PET ligand that identifies tau pathology in the brains of patients with AD. *Nat Rev Neurol.* 2013;9:599.
13. Waldeck DH. Photoisomerization dynamics of stilbene. *Chem Rev.* 1991;91: 415–436.
14. Fukumura T, Suzuki H, Mukai K, et al. Development of versatile synthesis equipment for multiple production of PET radiopharmaceuticals [abstract]. *J Labelled Comp Radiopharm.* 2007;50(suppl 1):S202.
15. Chen JJ, Huang SJ, Finn RD, et al. Quality control procedure for 6-[^{18}F]fluoro-L-DOPA: a presynaptic PET imaging ligand for brain dopamine neurons. *J Nucl Med.* 1989;30:1249–1256.
16. Yu S. Review of ^{18}F-FDG synthesis and quality control. *Biomed Imaging Interv J.* 2006;2:e57.
17. Jung JC. In-process 20-minute endotoxin "limit test" for positron emission tomography radiopharmaceuticals. *J Am Pharm Assoc.* 2006;46:89–92.
18. Channing MA. Analysis of residual solvents in 2-[^{18}F]FDG by GC. *Nucl Med Biol.* 2001;28:469–471.
19. Takei M, Kida T, Suzuki K. Sensitive measurement of positron emitters eluted from HPLC. *Appl Radiat Isot.* 2001;55:229–234.
20. Wilson AA, Garcia A, Chestakova A, et al. A rapid one-step radiosynthesis of the β-amyloid imaging radiotracer *N*-methyl-[^{11}C]2-(4′-methylaminophenyl)-6-hydroxybenzothiazole ([^{11}C]-6-OH-BTA-1). *J Labelled Comp Radiopharm.* 2004;47:679–682.
21. Andersson JD, Varnas K, Cselenyi Z, et al. Radiosynthesis of the candidate β-amyloid radioligand [^{11}C]AZD2184: positron emission tomography examination and metabolite analysis in cynomolgus monkeys. *Synapse.* 2010;64:733–741.
22. Scheinin NM, Tolvanen TK, Wilson IA, et al. Biodistribution and radiation dosimetry of the amyloid imaging agent ^{11}C-PIB in humans. *J Nucl Med.* 2007;48:128–133.
23. Xia CF, Arteaga J, Chen G, et al. [^{18}F]T807, a novel tau positron emission tomography imaging agent for Alzheimer's disease. *Alzheimers Dement.* 2013;9:666–676.

The Journal of NUCLEAR MEDICINE

Radiosynthesis, Photoisomerization, Biodistribution, and Metabolite Analysis of ^{11}C-PBB3 as a Clinically Useful PET Probe for Imaging of Tau Pathology

Hiroki Hashimoto, Kazunori Kawamura, Nobuyuki Igarashi, Makoto Takei, Tomoya Fujishiro, Yoshiharu Aihara, Satoshi Shiomi, Masatoshi Muto, Takehito Ito, Kenji Furutsuka, Tomoteru Yamasaki, Joji Yui, Lin Xie, Maiko Ono, Akiko Hatori, Kazuyoshi Nemoto, Tetsuya Suhara, Makoto Higuchi and Ming-Rong Zhang

J Nucl Med. 2014;55:1532-1538.
Published online: June 24, 2014.
Doi: 10.2967/jnumed.114.139550

The Journal of Nuclear Medicine is published monthly.
SNMMI | Society of Nuclear Medicine and Molecular Imaging
1850 Samuel Morse Drive, Reston, VA 20190.
(Print ISSN: 0161-5505, Online ISSN: 2159-662X)

SNMMI SOCIETY OF NUCLEAR MEDICINE AND MOLECULAR IMAGING